OncoTargets and Therapy

Dovepress
open access to scientific and medical research

Open Access Full Text Article

ORIGINAL RESEARCH

Preparation and SPECT/CT Imaging of ^{177}Lu-Labeled Peptide Nucleic Acid (PNA) Targeting CITED1: Therapeutic Evaluation in Tumor-Bearing Nude Mice

This article was published in the following Dove Press journal:
OncoTargets and Therapy

Jia Li
Lei Zhang
Wenbo Li
Chengming Lei
Yiyi Cao
Ying Wang
Zhengjie Wang
Hua Pang

Department of Nuclear Medicine, The First Affiliated Hospital of Chongqing Medical University, Chongqing, People's Republic of China

Purpose: The expression of Cbp/p300-interacting transactivator with Glu/Asp-rich carboxy-terminal domain 1 (CITED1) is upregulated in papillary thyroid carcinoma (PTC) and mediates cell proliferation and migration. To facilitate early diagnosis and monitoring of recurrent or metastatic PTC, we designed ^{177}Lu-labeled antisense peptide nucleic acid (PNA) targeting CITED1 mRNA to evaluate the therapeutic potential, while analyzing its distribution in nude mice and the characteristics withsingle-photon emission-computed tomography/computed tomography (SPECT/CT) imaging.

Materials and Methods: ^{177}Lu-DOTA-anti-CITED1-PNA (^{177}Lu-asPNA) was obtained by indirect labeling. High-performance liquid chromatography (HPLC) and thin-layer chromatography (TLC) were used to determine the labeling rate and radiochemical purity. The stability of ^{177}Lu-asPNA was evaluated by TLC, and the radioactivity count was measured by a γ counter to calculate its uptake capacity in K1 cells. To analyze the distribution of ^{177}Lu-asPNA in body tissues and organs of nude mice, static single-photon emission-computed tomography (SPECT) imaging and SPECT/CT image fusion were performed. Then, the therapeutic effects of probes were explored by tumor growth curves and survival analysis.

Results: Our probe showed a radiochemical purity of 96.5±0.15% at 1 hr and specific activity of 8.7±0.53 MBq/μg. The uptake rate in the ^{177}Lu-asPNA group was much higher than that in the ^{177}Lu-DOTA-nonsense-PNA (^{177}Lu-nonsense-PNA) and ^{177}Lu-DOTA groups ($P<0.05$). The biological distribution showed that the tumor/muscle ratio was at its highest at 24 h (4.98±0.34) post-inoculation, with SPECT/CT imaging showing clear tumor development. By measuring tumor volume of tumor-bearing nude mice, the ^{177}Lu-asPNA group showed a significant difference in tumor size 9 days after injection ($P < 0.05$). Kaplan-Meier survival curves showed that the overall survival rate in the ^{177}Lu-asPNA group was significantly different from those in the DOTA-anti-CITED1-PNA (asPNA) and saline groups ($P = 0.002$, log-rank test).

Conclusion: ^{177}Lu-asPNA was developed successfully, showing a high labeling rate and good stability. SPECT/CT imaging demonstrated tumor growth in nude mice, which was effectively inhibited by our probe, thus prolonging survival.

Keywords: antisense therapy, SPECT/CT imaging, papillary thyroid carcinoma, diagnosis and treatment integration

Correspondence: Hua Pang; Zhengjie Wang
Department of Nuclear Medicine, The First Affiliated Hospital of Chongqing Medical University, No. 1 Youyi Road, Chongqing 400016, People's Republic of China
Tel +8615923039337; +8618581493111
Email phua1973@163.com; bkzg1234@163.com

Introduction

Papillary thyroid carcinoma (PTC) constitutes almost 80% of all pathological cases of thyroid cancer.[1] Although the prognosis is generally good, it has been reported that 25% of the subjects will ultimately experience lymph node metastasis and

postoperative recurrence,[2,3] with some dying due to disease progression.[4] Currently, fine-needle aspiration biopsy (FNAB) is recommended for the diagnosis of thyroid nodules, with the routine treatment being surgery and radioactive iodine. However, due to limitations associated with the puncture site and biopsy collection method, about 20% of the thyroid nodules cannot be clearly diagnosed.[5–7] In addition, some patients exhibit degenerative changes in tumor cells and function during the disease course, reducing the benefits conferred by ^{131}I treatment.[8,9] Therefore, a non-invasive, specific diagnostic method combined with an effective molecular marker for targeted therapy is required for PTC.

At present, the sensitivity and specificity of preoperative genetic screening for thyroid cancer molecular markers (such as classic BRAF^{V600E}) in predicting PTC are about 70% and 80%, respectively, making it difficult to accurately predict the malignancy and prognosis.[10,11] Preclinical studies have demonstrated that the expression of Cbp/p300-interacting transactivator with Glu/Asp-rich carboxy-terminal domain 1 (CITED1) in PTC was significantly up-regulated,[12,13] thus promoting PTC cell proliferation, migration, and invasion.[14] In recent years, the rapid development of molecular imaging and radiopharmaceuticals has led to the establishment of anti-gene therapy as a viable therapeutic strategy.[15] Peptide nucleic acid (PNA) was developed from oligonucleotides (ODN), which can block the function of RNA polymerase structurally and thus interferes with gene transcription and down-regulates the expression of target genes.[16] Compared to ODN, PNA has the characteristics of easy absorption, strong specificity and high stability, which may facilitate the treatment of tumors and blood diseases. Therefore, blocking CITED1 expression by an antisense PNA (asPNA) binding CITED1 mRNA may be one of the effective methods for the diagnosis and treatment of iodine resistance to PTC.[17] However, in addition to using chemically modified PNA, radionuclide-coupled PNA also can enhance its lethality to some extent through synergistic effects.[18,19]

Studies have been reported PNA labeled with ^{99m}Tc for imaging endogenous gene expression in breast cancer, showing the broad prospect of combining peptide nucleic acids with nuclides in the diagnosis of diseases by tumor imaging.[20] Considering the unique properties of PNA, including resistance to enzymatic digestion, inhibition of gene expression of interest appears to be an effective method of cancer treatment.[21] Different from ^{99m}Tc, ^{177}Lu is a long half-life (6.7d) nuclide that can simultaneously emit β-particles and γ-rays for targeted radionuclide therapy (TRT) and single-photon emission computed tomography (SPECT).[22] For patients who are not susceptible to conventional 131-iodine therapy or who have distant metastases, ^{177}Lu may constitute a good alternative nuclide for the treatment of iodine-insensitive PTC. Due to the proneoplasticity and micro-penetration of ^{177}Lu, it can be used to detect tumors in patients with iodine insensitivity and inflicts radiation damage on tumors without damaging healthy bone marrow tissue.[23] In this study, ^{177}Lu-labeled antisense PNA was used to block the expression of CITED1 in K1 cells and a PTC xenograft model compatible with SPECT/CT imaging was used to evaluate its therapeutic potential.

Materials and Methods

Cell Culture and Establishment of Nude Mouse Model

K1 Cells were purchased from the Cell Bank at Shanghai Institute of Cell Biology, Chinese Academy of Science (Shanghai, China). K1 Cells were grown in Dulbecco's modified eagle medium (DMEM) supplemented with 10% fetal bovine serum (FBS) (both from Gibco, Thermo Fisher Scientific, Waltham, MA, USA) at 37°C in humidified atmosphere containing 5% CO_2, cells in the logarithmic phase of growth were used for all experiments.

All animal experiments have been approved by the Guidelines of Chongqing medical University Biomedical Ethics Committee (Ethics number 2019–190). K1 cells (5×10^6, 100 μL) were inoculated subcutaneously into the right forelimb of female nude mice, the animals were used for Biodistribution and SPECT/CT imaging studies when the tumor volume reached >1 cm^3. At the same time, when the volume of tumors is larger than 0.05 cm^3, the efficacy evaluation experiment is performed.

Radiolabeling, Radiochemical Purity and Stability Test

PNA (CITED1 (NC_000023.11) sequence:5′-TAGTGCAG AA-3′) was synthesized by Beijing Saibaisheng Gene Technology Co., Ltd. PNA was labeled by ^{177}Lu according to previous studies.[18] In brief, 185 MBq of ^{177}Lu in 50 μL of ammonium acetate (0.2 mmol/L, pH = 5.0), containing approximately 1 mg/mL of gentisic acid and 0.1% Tween-80 was added to 50 μL asPNA/nonsense-PNA (20 μg). The reaction mixture was incubated at 90°C for 30 min, with continuous mixing. The reaction was stopped by adding 10 mmol/L

diethylenetriamine pentaacetic acid (DTPA; pH = 6) and thoroughly mixed by incubating for 5 min at room temperature. To increase the labeling rate of the metal ion ^{177}Lu, the solvent used was prepared with ultrapure water (18.2 MΩ.cm, 25°C) and deionized using Chelex-100. The Radiolabeling method of ^{177}Lu-DOTA as fellow: 37 MBq of ^{177}Lu in 50 μL of sodium acetate (30 mmol/L, pH = 5.0) was incubated with 1 mg of DOTA at 90°C for 30 min.

The labeling rate and radiochemical purity were determined as follows. Thin-layer chromatography (TLC) plates were developed with saline and acetone (Volume ratio 1:1), and radio-TLC detection was done using an AR-2000 TLC imaging scanner (Bioscan, Washington DC, USA). High-performance liquid chromatography (HPLC) was performed on a C-18 chromatographic column (4.6 mm × 250 mm; Waters, Milford, MA, USA) using a UV detector (λ260 nm; flow rate, 1 mL/min). Solvent A was a 0.1% trifluoroacetic acid (TFA)/H_2O solution and solvent B was a 0.1% TFA/acetonitrile solution. The elution gradient was 0~50% (30 min). The labeling rate and radiochemical purity of ^{177}Lu-asPNA and ^{177}Lu-nonsense-PNA were determined by TLC and HPLC, and ^{177}Lu-DOTA's was determined by TLC.

The purified probes were tested for stability at room temperature, and in human serum, at 1, 4, 12, 24, and 48 hrs. Specific activity (MBq/μg) was calculated according to the following formula: [^{177}Lu total radioactivity (MBq) × labeling rate (%)]/asPNA mass (μg).

In vitro Uptake and Retention Assay

For the uptake experiments, probes are divided into ^{177}Lu-asPNA targeted to CITED1, ^{177}Lu-nonsense-PNA whose sequences are non-homologous with CITED1 in Basic Local Alignment Search Tool (Blast), and ^{177}Lu-DOTA as blank control. K1 cells were seeded at 6 × 10^5 cells/well in 6-well plates (5 wells/group). When K1 cells were in logarithmic growth, 30 μL of ^{177}Lu-asPNA, ^{177}Lu-nonsense-PNA and ^{177}Lu-DOTA was added, respectively, followed by culture for 2, 4, 6, or 8 hrs. The top layer of liquid was collected into test tubes; cells were digested and precipitants were collected. The formula for cellular uptake (%) is as follows: precipitation/(supernatant + precipitation).

For retention studies, 30 μL of three probes mentioned above was added to each well with K1 cells, followed by culture for 6 hrs in an incubator. Culture media was replaced, cells were placed back into the incubator, and culture was continued for 2, 4, 6, and 8 hrs to collect supernatants and precipitants. The radioactivity of K1 cells was calculated using a γ-counter (Capintec, Ramsey, NJ, USA). The formula for cellular retention (%) is as follows: precipitation/(supernatant + precipitation).

Biodistribution Studies

Nude mice were randomly divided into four groups according to sacrifice time (n = 3/group). Each mouse was injected with 100 μL ^{177}Lu-asPNA (1.85 MBq) via the tail vein. Mice were sacrificed at 4, 12, 24, and 48 hrs, and blood, tumors, and heart, liver, spleen, lung, kidney, stomach, intestine, brain, bone, and muscle tissues were weighed and evaluated using the γ-counter. The percentage of injected dose per gram of tissue (%ID/g) was calculated as follows: %ID/g = tissue radioactivity count/(radioactivity count of injected drug × tissue mass) × 100%.

SPECT/CT Imaging

Nude mice were injected with 100 μL of ^{177}Lu-asPNA (37 MBq) and placed in the prone position on a rat plate. Dual-probe SPECT/CT imaging (SPECT/CT Symbia T2; Siemens, Germany) was performed at 4, 12, 24, 48 hrs after drug administration. The target/non-target (T/NT) value was calculated based on the region of interest (ROI) and SPECT/CT image fusion was done when the tumor image was most clear. The SPECT acquisition conditions were as follows: high-energy collimation; energy peaks of 113 and 208 keV; and matrix is 256 × 256. Scans were acquired over a 10-min period.

Therapeutic Evaluation

Mice with tumors larger than 0.05 cm^2 were randomly divided into three groups (n = 5). Every 4 days, 100 μL ^{177}Lu-asPNA (11.1 MBq/5 μg), asPNA (5 μg) or 0.9% saline was injected into the tail vein three times depending on the group assignment. Following the injections, the growth status, body weight, and tumor size of the three groups were observed at the same time every day. The effect of ^{177}Lu-asPNA on tumor-bearing mice was observed continuously for 45 days. Tumor size was calculated by the following formula: a × b^2/2, where a is the long diameter of the tumor and b is the short diameter of the tumor.

Statistical Methods

All experimental data were analyzed using the statistical software SPSS 22.0 (IBM Corp., Armonk, NY, USA), and each experiment was repeated 3 times independently. The measurement data were expressed by X±S, a Student's

t-test was used for the comparison of two sample means, the comparison between the mean of multiple groups was analyzed by one-way ANOVA, repeated measurement variance analysis was used to compare tumor growth curves, and nonparametric logarithmic rank (Log-rank) test was used to compare the distribution of two or more survival curves, a value of $P < 0.05$ was considered significant.

Results

Radiolabeling, Radiochemical Purity and Stability Test

PNA was labeled successfully with ^{177}Lu using an indirect labeling method. Figure 1A shows the chemical formula for DOTA-anti-CITED1-PNA. The TLC data showed that the Rf value of ^{177}Lu-asPNA (Figure 1B) and ^{177}Lu-nonsense-PNA (Figure 1C) ranged from 0.9 to 1.0, while the Rf value of ^{177}Lu-DOTA (Figure 1D) is around 0.8. The radiochemical purity of ^{177}Lu-asPNA (Figure 1E) and ^{177}Lu-nonsense-PNA (Figure 1F) was 96.5 ± 0.15% and 95.8 ± 0.57% according to HPLC. Due to the close linkage between metal and chelating agent marking and high marking rate. Due to the close binding of metal and chelating agent, the labeling rate of ^{177}Lu-DOTA was >98%, so HPLC was not used to detect the radiochemical purity.

Figure 2 shows the radiochemical purity of three groups of probes after storage at room temperature and serum at different time points. The labeling rate of ^{177}Lu-asPNA and ^{177}Lu-nonsense-PNA was above 91% at both room temperature and in human serum, indicating that both probes have good stability in vivo and in vitro. The radiochemical purity of ^{177}Lu-DOTA has been lower than 90% at 48 hrs, which may be related to the absence of the radiation protection agent gentisic acid during the labeling process.

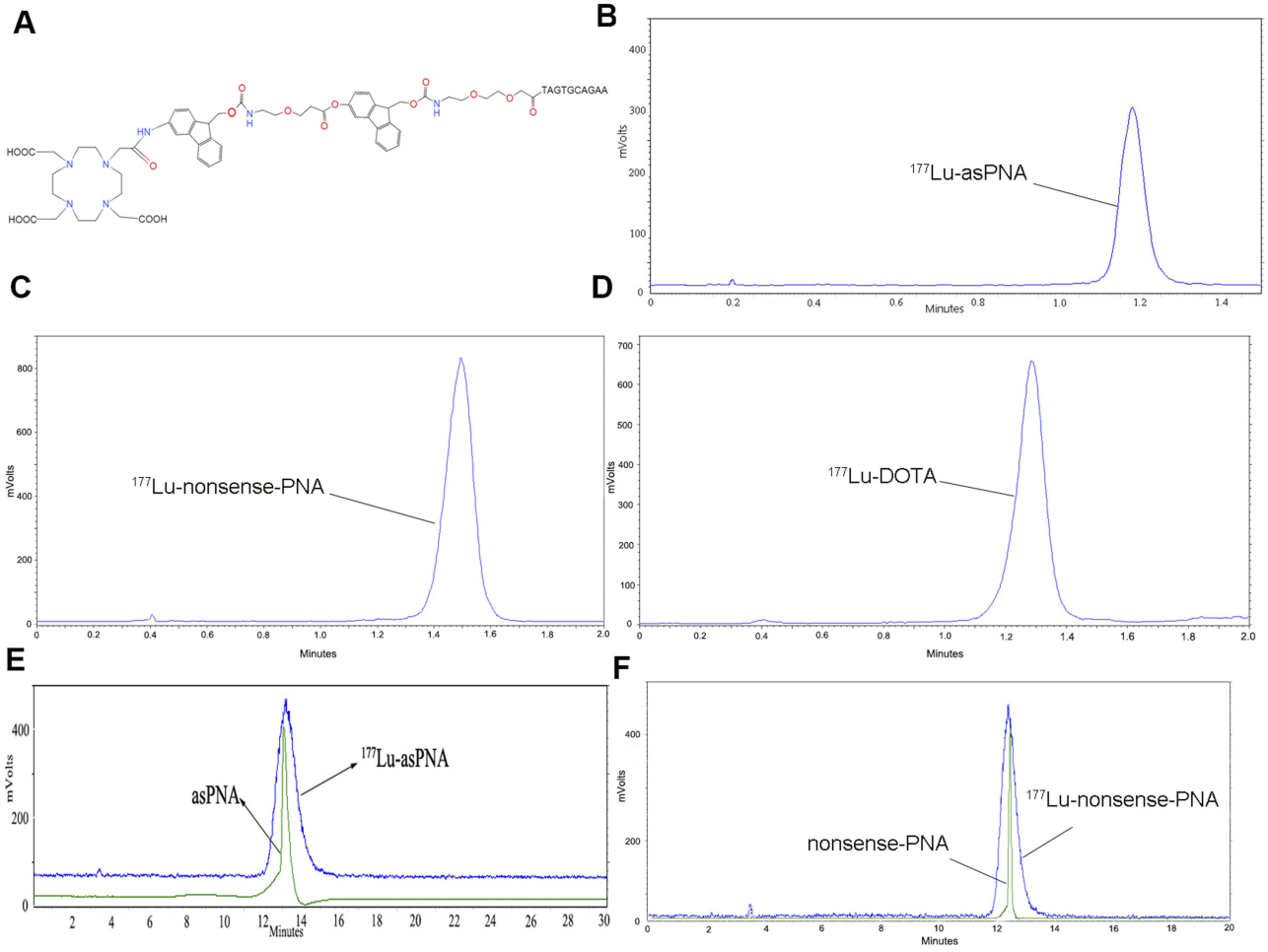

Figure 1 (**A**) the chemical formula for DOTA-anti-CITED1-PNA (asPNA; MW: 3452.4). The TLC data of ^{177}Lu-asPNA (**B**), ^{177}Lu-nonsense-PNA (**C**) and ^{177}Lu-DOTA (**D**); HPLC analysis of ^{177}Lu-asPNA with asPNA (**E**) and HPLC analysis of ^{177}Lu-nonsense-PNA with nonsense-PNA (**F**).

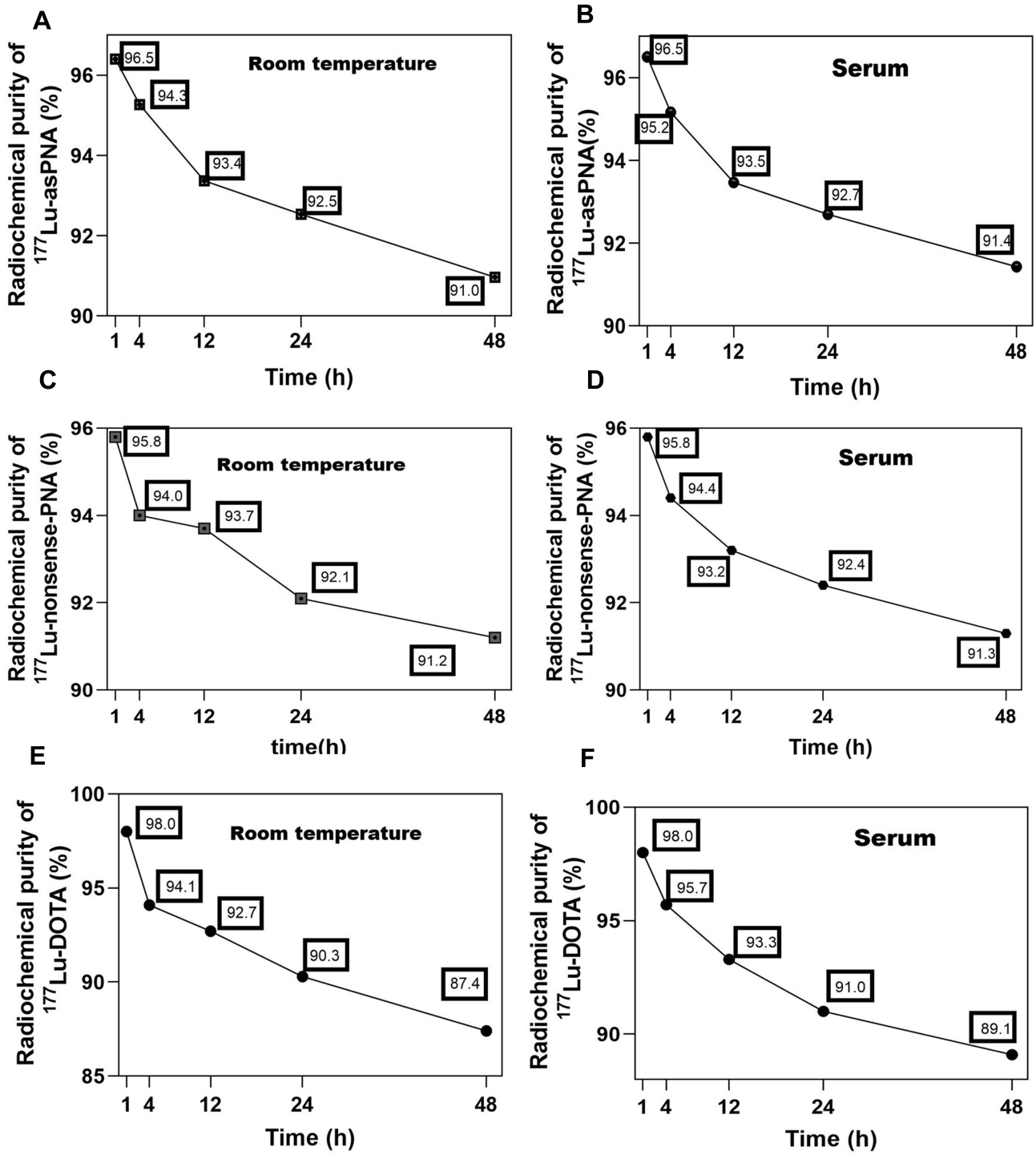

Figure 2 The room temperature and serum stability test of ^{177}Lu-asPNA (**A, B**), ^{177}Lu-nonsense-PNA (**C, D**) and ^{177}Lu-DOTA (**E, F**); specific radiochemical purity values for 1, 4, 12, 24, and 48 hrs are given here.

In vitro Uptake and Retention Assay

As shown in Figure 3A, the ^{177}Lu-asPNA and ^{177}Lu-nonsense -PNA gradually increased within the first 6 hrs, with peak uptake rates at 6 hrs of 8.59 ± 0.62% and 3.32 ± 0.22%, respectively. The uptake rate of the ^{177}Lu-asPNA group at each time point was significantly higher than that of the ^{177}Lu-nonsense-PNA($P<0.01$) and ^{177}Lu-DOTA groups at all time points ($P<0.001$).

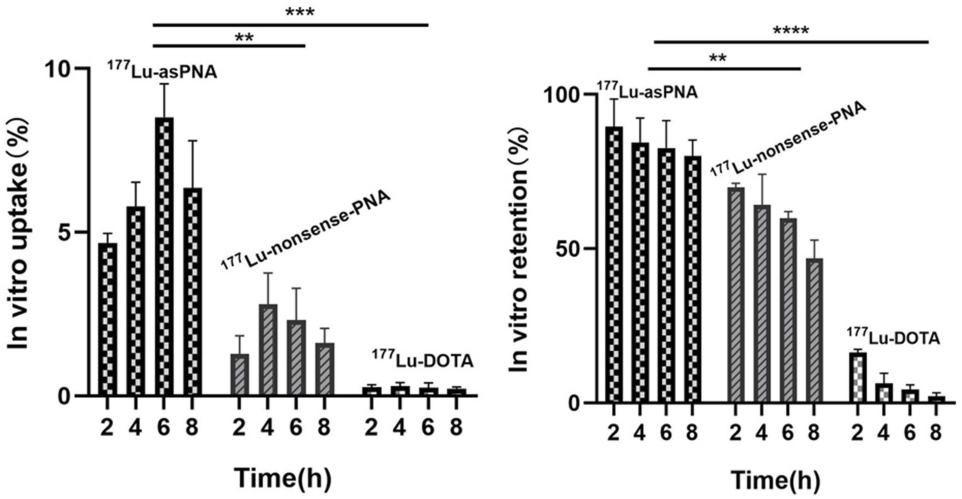

Figure 3 In vitro analysis of uptake (**A**) and retention (**B**) levels in K1 cells after treatment with ^{177}Lu-asPNA, ^{177}Lu-nonsense-PNA and ^{177}Lu-DOTA, respectively, at 2, 4, 6, and 8 hrs. **P<0.01, ***P<0.001, ****P<0.0001, compared with ^{177}Lu-asPNA group.

Cell retention experiments (Figure 3B) demonstrated that ^{177}Lu-asPNA and ^{177}Lu-nonsense-PNA undergo rapid removal between 0 and 2 hrs, followed by a slow decrease in the retention rate. The removal rate was significantly higher in the ^{177}Lu-nonsense-PNA (P<0.01) and ^{177}Lu-DOTA groups (P<0.0001) than the ^{177}Lu-asPNA group. This indicates that ^{177}Lu-asPNA is specifically taken up by K1 cells, and remains in these cells for an extended period of time.

Biodistribution Studies

Four weeks after injecting K1 cells, a nude mouse model of PTC was established. The biodistribution data are shown in Table 1. Radioactivity was high within the tumor tissues, liver, spleen, kidney, and blood at 4 hrs after injection. The liver and kidneys showed the highest radioactivity uptake, suggesting that these are the major organs involved in radioactive marker metabolism. No significant radioactive marker uptake in brain tissue was seen, indicating that the drug could not cross the blood-brain barrier. Tumor/Blood value showed a ratio of about 2.5 at 24 hrs and 48 hrs. Previously, the ratios were less than 1 due to the long accumulation of probes in the blood pool. There was no significant decrease in the tumor ^{177}Lu-labeled PNA concentration and the Tumor/Muscle value was highest in the tumor of 4.98 at 24 hrs.

Table 1 Biodistribution (%ID/g) of ^{177}Lu-asPNA in Tumor-Bearing Nude Mice (n=3)

Tissue	4h	12h	24h	48h
Blood	9.45±1.10	5.76±0.46	1.98±0.41	1.77±0.99
Lung	4.21±0.27	1.86±0.87	1.66±0.52	1.07±0.41
Heart	3.67±0.82	3.33±0.25	1.53±0.36	0.54±0.39
Liver	13.2±1.26	2.42±0.13	1.81±0.41	1.53±0.23
Spleen	10.96±1.07	4.62±0.58	2.07±0.62	1.14±0.14
Kidney	13.83±1.46	5.96±1.32	2.06±0.49	0.87±0.41
Stomach	4.92±0.26	2.34±0.42	2.05±1.03	0.58±0.27
Intestines	4.92±0.45	3.17±1.50	3.03±0.87	0.85±0.27
Bone	2.58±0.63	1.51±0.55	1.03±0.68	0.52±0.23
Brain	1.53±0.68	0.42±0.36	0.39±0.77	0.33±0.59
Muscle	2.13±0.37	1.21±0.69	0.99±0.21	0.75±0.18
Tumor	5.78±0.87	5.47±1.03	4.93±0.47	3.05±0.66
Tumor/Blood	0.61±1.24	0.95±0.97	2.49±1.33	2.65±0.73
Tumor/Muscle	2.71±0.28	4.52±0.69	4.98±0.34	4.06±0.22

SPECT/CT Imaging

The ability of ^{177}Lu-asPNA to detect K1 xenografts in vivo by SPECT/CT was also investigated. Prominent uptake of ^{177}Lu-asPNA was observed in the liver and kidneys, suggesting that the probes used are mainly excreted through the hepatobiliary route. Some ^{177}Lu-asPNA was present in the tumor tissue at 4 hrs, along with a gradual decrease of liver and kidney radioactivity. Tumor and muscle tissue probe concentrations were highest at 24 hrs, and the highest T/NT value was 5.11 (Figure 4A). At this timepoint, the SPECT/CT fusion tumor image was most clear (Figure 4B). At 48 hrs, the probe concentration in the tumor had decreased only slightly.

Therapeutic Evaluation

Figure 5A compares tumor size changes over 24 days after treatment among the groups. A difference in tumor volume among the groups was noted at 9 days after injection (P < 0.05). Eighteen days after injection, the tumor growth rate and volume of the ^{177}Lu-asPNA group was much lower than that

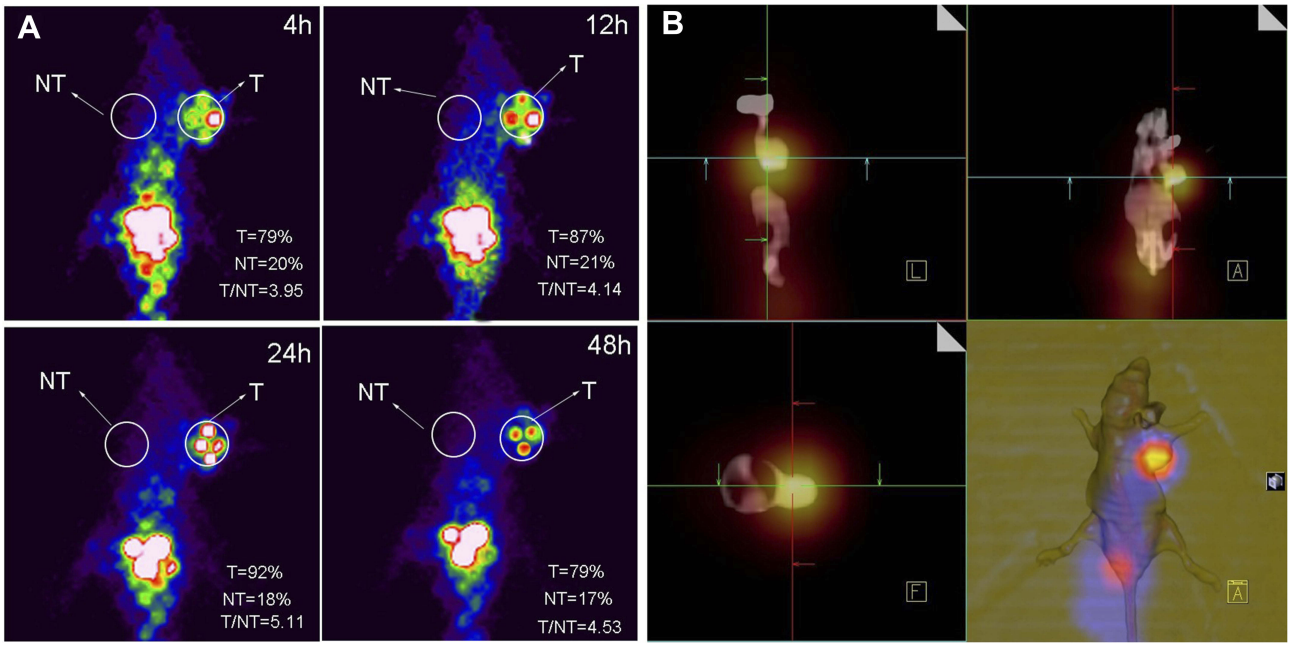

Figure 4 Static SPECT imaging and SPECT/CT fusion imaging. (**A**) SPECT imaging of a tumor-bearing mouse after the tail vein injection of ^{177}Lu-asPNA was acquired at 4, 12, 24, and 48 hrs. (**B**) The sagittal, coronary, axial images and simulation images of SPECT/CT fusion imaging of tumor-bearing mice at 24 hrs after the injection of ^{177}Lu-asPNA into the tail vein.

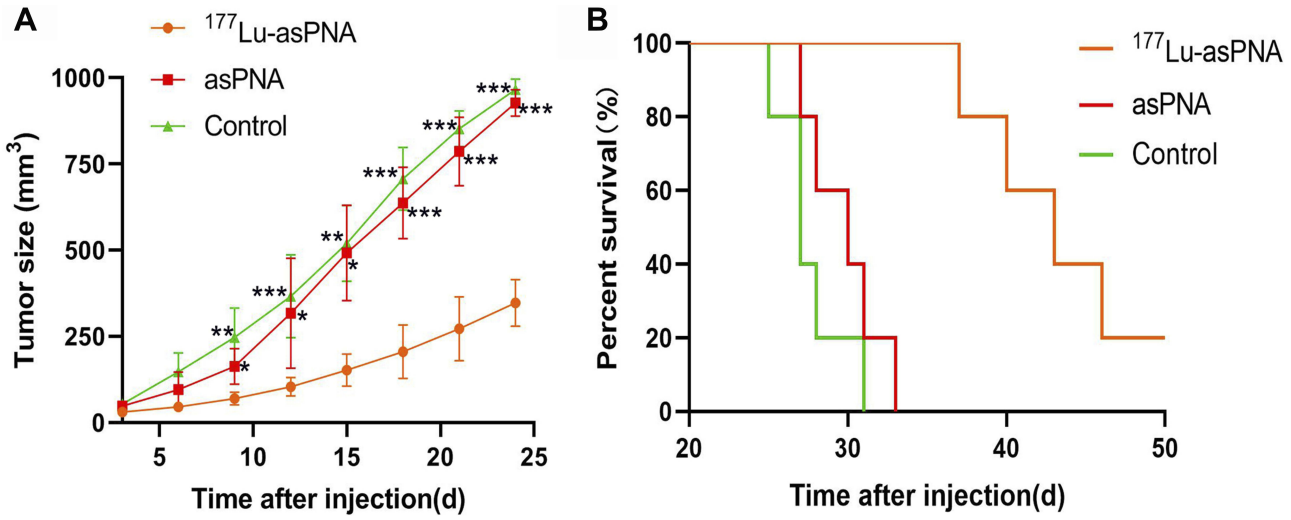

Figure 5 (**A**) Comparison of the size of tumor volume within 24 days treatment in ^{177}Lu-asPNA, asPNA and saline groups. *P<0.05, **P<0.01, ***P<0.001, compared with the group of ^{177}Lu-asPNA. (**B**) The comparison of Kaplan-Meier survival curve of three groups of tumor-bearing mice after treatment.

of the asPNA and saline groups. The tumor volume of the asPNA group was lower than that of the saline group, but not significantly ($P > 0.05$). These results show that the ^{177}Lu-asPNA can effectively inhibit tumor growth in nude mice. Figure 5B shows the survival curve of each treatment group, with a median survival time of the ^{177}Lu-asPNA, asPNA and saline groups as 43 days, 30 days, and 27 days, respectively. The overall survival rate of the ^{177}Lu-asPNA group was significantly higher than that of the asPNA groups ($P = 0.002$, Log-rank test) and saline groups ($P = 0.002$, Log-rank test). Taken together, these results indicate that ^{177}Lu-asPNA can effectively prolong the survival of tumor-bearing nude mice.

Discussion

The pathogenesis of iodine-refractory thyroid cancer is associated with mutations in BRAF and RAS genes, rearrangement of RET/PTC and PAX8/PPAR chromosomes,

and activation of MAPK and PI3K/AKT signaling pathways.[8,9,24] $BRAF^{V600E}$ is the most common type of mutation, which is thought to be seen only in PTC, but the detection of $BRAF^{V600E}$ depends on the accurate location of thyroid fine needle aspiration.[25,26] Prasad et al confirmed by RT-PCR and immunohistochemistry that CITED1 expression in PTC was significantly up-regulated and could promote the proliferation of thyroid papillary cancer cells by regulating related pathways.[27] *S*ubsequently, several scholars confirmed that the expression of CITED1 in thyroid papillary carcinoma was much higher than that in normal thyroid tissue.[28,29] These indicate that CITED1 has potential application value in differentiating PTC from benign thyroid lesions. In this study, we showed that ^{177}Lu-labeled PNA can specifically aggregate in papillary thyroid carcinoma, and can effectively inhibit tumor growth and prolong the life cycle of nude mice. We successfully developed a molecular probe with a labeling rate of 94.7±0.83%, radiochemical purity of 96.5±0.15% at 1 hr, and specific activity of 8.7±0.53 MBq/μg. After incubation at room temperature and in human serum, the radiochemical purity of the probe remained above 91% at 48 hrs. The uptake rate of antisense PNA reached a peak of 8.59% at 6 hrs, which was 5.27% higher than that of the nonsense PNA group. The tumor/muscle radiation count peaked at 4.98 after 24 hrs, consistent with the T/NT ratio of 5.11 seen at the optimal timepoint for SPECT/CT imaging. After 18 days of treatment, the average tumor volume of the ^{177}Lu-asPNA group was about two-fold smaller than that of the asPNA and saline groups, and the median survival time of the ^{177}Lu-asPNA group was at least 13 days longer than those of the other two groups.

Since PNA is not negatively charged, there is no electrostatic repulsion between DNA and RNA, PNA is more effective than ODN in binding to the mRNA of a target gene.[21] Against this background, we designed an anti-CITED1-PNA that was complementary to the first 10 codons of the open reading frame of CITED1 mRNA. This probe stimulates degradation of CITED1 mRNA and inhibits further protein synthesis. In this study, to ensure high water solubility, we controlled the content of purines in PNA sequence below 60% and added up to three consecutive purines in the probe; to increase absorption and stability, PNA was modified with O-O linkers.[17,30,31] We then used ^{177}Lu to label PNA with a chelating agent 1,4,7,10- tetraazacyclododecane-N, N', N, N'-tetraacetic acid (DOTA), the PNA sequence is combined with DOTA and can be incorporated into any position of the peptide-PNA coupling and incorporated into the peptide that mediates cell penetration and PNA internalization.[32,33] In cell internalization experiments, the uptake rate of the ^{177}Lu-nonsense-PNA group also increased slightly in the cellular uptake and retention experiments. It may be that ^{177}Lu-nonsense-PNA has a certain non-specific binding in K1 cells, which is why the retention rate of ^{177}Lu-nonsense-PNA has decreased so quickly. In addition, after 8 hrs, the uptake of ^{177}Lu-asPNA showed a downward trend. Combined with the results of studies, it was shown that with the short-term decrease in time, the cellular uptake of PNA tended to rise and I think this may indicate that the process of PNA uptake by cells is not a simple process of removing markers from cells, but may be a gradual process. It can be seen that higher cell uptake rate and slower cell clearance rate are specific manifestations of antisense peptide nucleic acid in K1 cells, which support the conclusion that antisense PNA can be used to modulate the transcription and translation of tumor genes, and that their high stability and strong binding affinity make these molecules useful for detecting tumor cells.[16,34]

Preclinical studies of ^{68}GA-labeled ODNs for pulmonary malignancies have been designed to target the activated human K-ras oncogene;[35] an increasing number of prospective studies have begun to apply antisense therapy using ^{125}I or ^{111}In in patients with central nervous system and cervical cancers.[36–38] This study once again confirmed the feasibility of antisense imaging and further explored the efficacy of antisense therapy using ^{177}Lu coupling, which is based on study showed that PNA can be metabolized in cells over several months.[39] In vivo probe distribution and imaging results were consistent with previous studies reporting PNA aggregation in tumor sites.[40] In nude mice distribution, a high tumor/blood ratio can be achieved only 24 hrs, due to the continuous concentration of ^{177}Lu-asPNA in the blood pool within 12 hrs. This trend of slow elimination from the blood pool is also visible looking at the heart and muscle activity. However, we believe that despite the slow metabolism of the blood pool, the radioactive concentration of the tumor gradually increases and a high tumor/blood ratio appears after 24 hrs. This result is consistent with the highest 24-hr tumor/muscle value, while the optimal time for imaging was previously reported as 48 hrs, our results indicated that it was closer to 24 hrs. A significant concentration of ^{177}Lu-labeled PNA remained in the tumor at 48 hrs(T/NT=4.53), indicating continuous tumor development. In addition, although the probe had a good imaging effect

on the tumor, with a T/NT ratio of 5.11, the slow excretion in the body was also significant, which reduced the contrast of the image to some extent. Therefore, in order to improve the gastrointestinal clearance rate, the available strategies include replacing the peptide nucleic acids modified only by O-O linker with neutral hydrophilic serine and aspartic acid residues. On the other hand, micro-PET /CT with higher resolution and sensitivity or using kidney blockers is also feasible.

At present, PTC is treated by a combination of surgical resection of the lesion, ^{131}I radiation for removal of residual thyroid, and inhibition of thyroid-stimulating hormone (TSH).[24] However, some patients exhibited de-differentiation during ^{131}I treatment, with the cells exhibiting progressive degeneration in morphology and function. Studies have shown that ^{131}I radiation can reduce the iodine uptake capacity of PTC cells, but decrease the mRNA and protein expression of sodium/iodide symporter (NIS) transporters.[41] ^{177}Lu has a half-life similar to ^{131}I and is also compatible with SPECT and TRT, thus solving the problem of insufficient iodine uptake by PTC cells; moreover, it could likely be applied to other tumors in the future. Based on our results, the use of ^{177}Lu-labeled PNA could pave the way to a new approach for diagnosing and treating iodine-refractory thyroid cancer. ^{177}Lu-labeled PNA had a positive effect with respect to inhibiting tumor volume and extending the life of nude mice; mice survived at a 38% and 36% higher rate than the other two groups, respectively. Our results were consistent with Boffa and colleagues, who used PNA to down-regulate c-myc in the treatment of cancer, thus suggesting the high potential of PNA for cancer therapy.[42]

In conclusion, we successfully targeted CITED1 mRNA with ^{177}Lu-labeled antisense PNA, achieving a high labeling rate and stability. Moreover, we confirmed that PNA specifically accumulates in tumors, to inhibit the growth thereof and thus prolong the life cycle of nude mice. This suggests a possible alternative diagnostic and treatment modality for PTC patients, which may be especially useful for those showing no increase in iodine sensitivity after multiple treatments.

Acknowledgments

The authors gratefully acknowledge the assistance of the Department of Nuclear Medicine, First Affiliated Hospital of Chongqing Medical University, Institute of Radiation Oncology Laboratory and Animal Experiment Center of Chongqing Medical University. This work was supported by the Graduate Innovation Research Project of Chongqing (grant number CYS17152).

Disclosure

The authors report no conflicts of interest in this work.

References

1. Roman BR, Morris LG, Davies. L. The thyroid cancer epidemic, 2017 perspective. *Curry Opine EndocrinolDiabetes Lobes*. 2017;24 (5):332–336. doi:10.1097/MED.0000000000000359
2. Abdullah MI, Junit SM, Ng KL, et al. Papillary thyroid cancer: genetic alterations and molecular biomarker investigations. *Int J Med Sci*. 2019;16:450–460. doi:10.7150/ijms.29935
3. Siegel RL, Miller KD, Jemal A. Cancer statistics, 2018. *CA Cancer J Clin*. 2018;68:7–30. doi:10.3322/caac.21442
4. Brown RL, de Souza JA, Cohen EE. Thyroid cancer: burden of illness and management of disease. *J Cancer*. 2011;2:193–199. doi:10.7150/jca.2.193
5. Cheung CC, Ezzat S, Freeman JL, Rosen IB, Asa SL. Immunohistochemical diagnosis of papillary thyroid carcinoma. *Mod Pathol*. 2001;14:338–342. doi:10.1038/modpathol.3880312
6. Wu G, Wang J, Zhou Z, Li T, Tang F. Combined staining for immunohistochemical markers in the diagnosis of papillary thyroid carcinoma: improvement in the sensitivity or specificity? *J Int Med Res*. 2013;41:975–983. doi:10.1177/0300060513490617
7. Xing M, Tufano RP, Tufaro AP, et al. Detection of BRAF mutation on fine needle aspiration biopsy specimens: a new diagnostic tool for papillary thyroid cancer. *J Clin Endocrinol Metab*. 2004;89:2867–2872. doi:10.1210/jc.2003-032050
8. Gruber JJ, Colevas AD. Differentiated thyroid cancer: focus on emerging treatments for radioactive iodine-refractory patients. *Oncologist*. 2015;20:113–126. doi:10.1634/theoncologist.2014-0313
9. Schmidt A, Iglesias L, Klain M, Pitoia F, Schlumberger MJ. Radioactive iodine-refractory differentiated thyroid cancer: an uncommon but challenging situation. *Archiv Endocrinol Metab*. 2017;61:81–89. doi:10.1590/2359-3997000000245
10. Knauf JA, Ma X, Smith EP, et al. Targeted expression of BRAFV600E in thyroid cells of transgenic mice results in papillary thyroid cancers that undergo dedifferentiation. *Cancer Res*. 2005;65:4238–4245. doi:10.1158/0008-5472.CAN-05-0047
11. Liao T, Qu N, Shi RL, et al. BRAF-activated LncRNA functions as a tumor suppressor in papillary thyroid cancer. *Oncotarget*. 2017;8:238–247. doi:10.18632/oncotarget.10825
12. Li H, Guan H, Guo Y, et al. CITED1 promotes proliferation of papillary thyroid cancer cells via the regulation of p21 and p27. *Cell Biosci*. 2018;8:57–63. doi:10.1186/s13578-018-0256-9
13. Xia E, Wang Y, Bhandari A, et al. CITED1 gene promotes proliferation, migration and invasion in papillary thyroid cancer. *Oncol Lett*. 2018;16:105–112. doi:10.3892/ol.2018.8653
14. Wang Y, Huang H, Hu F, et al. CITED1 contributes to the progression of papillary thyroid carcinoma via the Wnt/beta-catenin signaling pathway. *Onco Targets Ther*. 2019;12:6769–6777. doi:10.2147/OTT.S215025
15. Lee HT, Kim SK, Yoon JW. Antisense peptide nucleic acids as a potential anti-infective agent. *J Microbiol*. 2019;57:423–430. doi:10.1007/s12275-019-8635-4
16. Sakai J, Maeda T, Tarumoto N, et al. A novel detection procedure for mutations in the 23S rRNA gene of Mycoplasma pneumoniae with peptide nucleic acid-mediated loop-mediated isothermal amplification assay. *J Microbiol Methods*. 2017;141:90–96. doi:10.1016/j.mimet.2017.08.009
17. Quijano E, Baha R, Ricciardi A, Saltzmanc WM. Therapeutic peptide nucleic acids: principles, limitations, and opportunities. *Yale J Biol Med*. 2017;90:7.

18. Balkin ER, Jia F, Miller WH, Lewis MR. In vitro evaluation of targeted antisense 177Lu radiotherapy. *Anticancer Res*. 2011;31:3143–3149.
19. Balkin ER, Liu D, Jia F, et al. Comparative biodistributions and dosimetry of [(1)(7)(7)Lu]DOTA-anti-bcl-2-PNA-Tyr(3)-octreotate and [(1)(7)(7)Lu]DOTA-Tyr(3)-octreotate in a mouse model of B-cell lymphoma/leukemia. *Nucl Med Biol*. 2014;41:36–42. doi:10.1016/j.nucmedbio.2013.10.006
20. Tian X, Aruva MR, Qin W, et al. Noninvasive molecular imaging of MYC mRNA expression in human breast cancer xenografts with a [99mTc]peptide-peptide nucleic acid-peptide chimera. *Bioconjug Chem*. 2005;16:70–79. doi:10.1021/bc0497923
21. Montazersaheb S, Hejazi MS. Potential of peptide nucleic acids in future therapeutic applications. *Adv Pharm Bull*. 2018;8:551–563. doi:10.15171/apb.2018.064
22. Calais PJ, Turner JH. Radiation safety of outpatient 177Lu-octreotate radiopeptide therapy of neuroendocrine tumors. *Ann Nucl Med*. 2014;28:531–539. doi:10.1007/s12149-014-0843-8
23. Alexander N, Vali R, Ahmadzadehfar H, Shammas A, Baruchel S. Review: the role of radiolabeled DOTA-conjugated peptides for imaging and treatment of childhood neuroblastoma. *Curr Radiopharm*. 2018;11:14–21. doi:10.2174/1874471011666171215093112
24. Jin Y, Van Nostrand D, Cheng L, Liu M, Chen L. Radioiodine refractory differentiated thyroid cancer. *Crit Rev Oncol Hematol*. 2018;125:111–120. doi:10.1016/j.critrevonc.2018.03.012
25. Kebebew E, Weng J, Bauer J, et al. The prevalence and prognostic value of BRAF mutation in thyroid cancer. *Ann Surg*. 2007;246:-466–470; discussion 470–461. doi:10.1097/SLA.0b013e318148563d
26. Xing M. BRAF mutation in thyroid cancer. *Endocr Relat Cancer*. 2005;12:245–262. doi:10.1677/erc.1.0978
27. Prasad ML, Pellegata NS, Kloos RT, et al. CITED1 protein expression suggests Papillary Thyroid Carcinoma in high throughput tissue microarray-based study. *Thyroid*. 2004;14:169–175. doi:10.1089/105072504773297830
28. Ding S, Qu W, Jiao Y, et al. LncRNA SNHG12 promotes the proliferation and metastasis of papillary thyroid carcinoma cells through regulating wnt/beta-catenin signaling pathway. *Cancer Biomarkers*. 2018;22:217–226. doi:10.3233/CBM-170777
29. Ihermann-Hella A, Hirashima T, Kupari J, et al. Dynamic MAPK/ERK Activity Sustains Nephron Progenitors through Niche Regulation and Primes Precursors for Differentiation. *Stem Cell Rep*. 2018;11:912–928. doi:10.1016/j.stemcr.2018.08.012
30. Liu C, Wang J, Zeng F. Cellular delivery of modified peptide nucleic acids: a review. *Chin J Biotechnol*. 2016;32:292–305.
31. Westerlund K, Honarvar H, Tolmachev V, Eriksson Karlstrom A. Design, preparation, and characterization of PNA-based hybridization probes for affibody-molecule-mediated pretargeting. *Bioconjug Chem*. 2015;26:1724–1736. doi:10.1021/acs.bioconjchem.5b00292
32. Pansuwan H, Ditmangklo B, Vilaivan C, et al. Hydrophilic and cell-penetrable pyrrolidinyl peptide nucleic acid via post-synthetic modification with hydrophilic side chains. *Bioconjug Chem*. 2017;28:2284–2292. doi:10.1021/acs.bioconjchem.7b00308
33. Karczmarczyk U, Wojdowska W, Mikolajczak R, et al. Influence of DOTA chelators on radiochemical purity and biodistribution of ^{177}Lu- and ^{90}Y-Rituximab in xenografted mice. *Iran J Pharm Res*. 2018;17:1201–1208.
34. D'Agata R, Giuffrida MC, Spoto G. Peptide nucleic acid-based biosensors for cancer diagnosis. *Molecules*. 2017;22:1951. doi:10.3390/molecules22111951
35. Roivainen A, Tolvanen T, Salomaki S, et al. 68Ga-labeled oligonucleotides for in vivo imaging with PET. *J Nucl Med*. 2004;45:347–355.
36. Panyutin IG. Labeling peptide nucleic acids with indium-111. *Methods Mol Biol*. 2019;1973:185–191.
37. Pradhan AA, Clarke PB. Pharmacologically selective block of mu opioid antinociception by peptide nucleic acid antisense in absence of detectable ex vivo knockdown. *Eur J Pharmacol*. 2005;506:229–236. doi:10.1016/j.ejphar.2004.11.018
38. Suzuki T, Zhang Y, Zhang YF, Schlachetzki F, Pardridge WM. Imaging gene expression in regional brain ischemia in vivo with a targeted [111in]-antisense radiopharmaceutical. *Mol Imaging*. 2004;3:356–363. doi:10.1162/1535350042973535
39. Kramer R, Mokhir A. Metal complex derivatives of peptide nucleic acids (PNA). *Met Ions Life Sci*. 2012;10:319–340.
40. Liu D, Balkin ER, Jia F, et al. Targeted antisense radiotherapy and dose fractionation using a ^{177}Lu-labeled anti-bcl-2 peptide nucleic acid-peptide conjugate. *Nucl Med Biol*. 2015;48:226–231. doi:10.3181/00379727-48-13279P
41. Rivera M, Ghossein R, Schoder H, et al. Histopathologic characterization of radioactive iodine-refractory fluorodeoxyglucose-positron emission tomography-positive thyroid carcinoma. *Cancer*. 2008;113:48–56. doi:10.1002/cncr.23515
42. Boffa LC, Cutrona G, Cilli M, et al. Therapeutically promising PNA complementary to a regulatory sequence for c-myc: pharmacokinetics in an animal model of human Burkitt's lymphoma. *Oligonucleotides*. 2005;15:85–93. doi:10.1089/oli.2005.15.85